Chemical Engineering Journal 147 (2009) 287–296

Contents lists available at ScienceDirect

Chemical Engineering Journal

journal homepage: www.elsevier.com/locate/cej

Highly effective synthesis of dimethyl carbonate from methanol and carbon dioxide using a novel copper–nickel/graphite bimetallic nanocomposite catalyst

Jun Bian[a], Min Xiao[a], Shuanjin Wang[a], Xiaojin Wang[a], Yixin Lu[b,*], Yuezhong Meng[a,**]

[a] State Key Laboratory of Optoelectronic Materials and Technologies, Institute of Optoelectronic and Functional Composite Materials, Sun Yat-Sen University, 135 Xingang West, Guangzhou 510275, PR China
[b] Department of Chemistry & Medicinal Chemistry Program, Office of Life Sciences, National University of Singapore, 3 Science Drive 3, Singapore 117543, Republic of Singapore

ARTICLE INFO

Article history:
Received 24 June 2008
Received in revised form 19 October 2008
Accepted 3 November 2008

Keywords:
Dimethyl carbonate
Carbon dioxide
Bimetallic catalyst
Catalysis

ABSTRACT

A novel graphite supported Cu–Ni bimetallic nanocomposite catalyst for direct synthesis of dimethyl carbonate (DMC) from CH_3OH and CO_2 has been synthesized and investigated. The support and the synthesized catalysts were fully characterized using BET surface area, TG–DSC, Raman spectra, FTIR, SEM–EDX, TEM, XRD, TPR and XPS techniques. The catalytic activities were investigated by performing micro-reactions. It has been found that the nitrogen adsorption isotherm of graphite oxide support showed a typical Type II features. The layered structure of graphite was well maintained in the synthesized catalysts. Metal particles with an average size of 15.8 nm were uniformly dispersed on the support surface. Metal phase and alloy phase of Cu and Ni in the catalyst were partially formed during the reduction and activation step. The Cu–Ni/graphite nanocomposite catalyst exhibited remarkably high activity, selectivity and stability for the direct synthesis of DMC. The highest DMC yield was higher than 9.0% at 378 K and 1.2 MPa and the selectivity of DMC was higher than 88.0%. The high catalytic activity of Cu–Ni/graphite nanocomposite catalyst in DMC synthesis could be attributed to the synergetic effects of metal Cu, Ni and Cu–Ni alloy in the activation of CH_3OH and CO_2, the unique structure of graphite and the interaction between the metal particles and the supports.

1. Introduction

Dimethyl carbonate (DMC) has attracted much attention in terms of a non-toxic substitute for dimethyl sulfide and phosgene that are toxic and corrosive as methylation or carbonylating agents [1–3]. Moreover, DMC is also considered to be an option for transportation fuels because of its high oxygen content (53.3%) and high octane value [4]. Several commercial processes have been developed for the synthesis of DMC, including methanolysis of phosgene [5], ester exchange process [1], carbon monoxide–methyl nitrite process [1] and gas-phase oxidative carbonylation of methanol [6]. However, all these processes use toxic, corrosive, flammable and explosive gases such as phosgene, hydrogen chloride and carbon monoxide. Therefore, direct synthesis of DMC from CH_3OH and CO_2 is highly desired since such an approach is environmentally benign by nature [1]:

$$2CH_3OH + CO_2 \rightarrow (CH_3O)_2CO + H_2O$$

Continuous emission of carbon dioxide (CO_2) into the atmosphere represents the main cause of greenhouse effect because of the stratospheric ozone depletion. Recently, it has been well recognized that the utilization of CO_2 is very important in terms of the utilization of carbon resource, synthesis chemistry and environment protection [7–9]. The possibility to convert CO_2 into environmentally friendly chemicals not only could limit the greenhouse environmental damages, but also constitutes a carbon source alternative to petroleum, natural gas and coal, that are all energetic resources destined to exhaust themselves. Besides, because of its large-scale availability at low cost, CO_2 could represent a precursor compound for the synthesis of useful chemical products, such as methanol, urea and salicylic acid. However, it is still a challenge for synthetic chemists to activate and utilize CO_2 effectively because of its highly thermodynamically stable and kinetically inert by nature.

* Corresponding author.
** Corresponding author. Tel.: +86 20 84114113; fax: +86 20 84114113.
E-mail address: mengyzh@mail.sysu.edu.cn (Y. Meng).

1385-8947/$ – see front matter © 2008 Elsevier B.V. All rights reserved.
doi:10.1016/j.cej.2008.11.006

In recent years, the direct synthesis of DMC from CH_3OH and CO_2 has attracted much attention in the view of the so-called "Sustainable Society" and "Green Chemistry". As a result, a great variety of catalysts have been checked to date at very different reaction conditions and with a variable degree of success. Wu et al. reported on direct synthesis DMC over H_3PO_4–V_2O_5 catalyst [10]. Under the optimal synthesis conditions, CH_3OH conversion only reached 1.9% with DMC selectivity of 88.0%. When Cu–Ni/VSO was used as a catalyst, DMC formation could reach 5.5 mmol with DMC selectivity of 87.0% under the given conditions [11]. Wang et al. reported 4.83% CH_3OH conversion and 87.2% DMC selectivity over the compound catalyst of Cu–(Ni,V,O)/SiO_2 with photo-assistance [12]. Besides, other catalyst systems have been reported to be effective in this reaction, including organometallic compounds [13], metal tetra-alkoxides [14], potassium carbonate [15], ZrO_2 [16,17], and $H_3PW_{12}O_4$–ZrO_2 [18]. Nevertheless, the yield of DMC obtained via one-step synthesis is still very low due to the difficulties in activation of CO_2 and due to the deactivation of catalysts by in situ produced water. Therefore, novel catalysts with high catalytic performance are required.

It is well known that support material plays an important role in the final catalyst. Selecting a suitable supporting material is a crucial factor to get highly effective catalysts. Graphite is a layered material having the thinnest atomic layer of all layered materials. Graphene sheets, one-atom-thick two-dimensional layers of sp^2-bonded carbon, are predicted to have a range of unusual properties. Recent studies have indicated that individual graphene sheets had extraordinary electronic transporting properties [19–22]. One possible route to harnessing these properties for applications would be to incorporate graphene sheets in a composite material, such as polymer/graphite and transition metal/graphite composites. Especially for transition metal/graphite composites having novel physical and chemical properties are very attractive for many organic reactions [23–25]. Richard and de Lopez-Gonzalez et al. reported that platinum and ruthenium particles supported on graphite gave higher selectivity towards unsaturated alcohol in the hydrogenation of cinnamaldehyde than the catalysts where the metals supported on other supports [25–26]. In these studies, it was proposed that the metal clusters were selectively located on the basal plane of the graphite, which led to a strong interaction between the metal particles and the π-electrons of the support medium. This was responsible for the observed differences in catalyst activity.

Transition metal/graphite composites have been studied intensively because these intercalation compounds are expected to exhibit new unique catalytic properties in many organic synthesis processes. However, because of the neutral properties of the graphite walls, there is no driving force strong enough for a rigid species to expand and prop the graphitic layers to form an open pore system, although the weak van der Waals-type bonding between the graphitic layers allows the formation of graphite intercalation compounds (GIC) for electrochemical/tribological application [27]. Graphite oxide (GO) is an oxygen-rich carbonaceous material, synthesized by the controlled oxidation of graphite. It shows excellent swelling/exfoliation properties similar to clay minerals [28–33]. In contrast to original graphite, the graphene derived sheets in GO (GO sheets) are heavily oxygenated, bearing hydroxyl and epoxide functional groups on their basal planes, in addition to carbonyl and carboxyl groups located at the sheet edges [30,31,34]. The presence of these functional groups makes graphene oxide sheets strongly hydrophilic, which allows GO to readily disperse in water to form stable colloidal suspensions via swelling and exfoliation [35]. Further, the GO shows unique absorption ability and acts as ion exchangers and metal ion binders [28,36]. Notably, it has been reported that graphite structure can be somewhat reduced after thermal treatment or chemical reduction of the GO [37]. Because of its particular properties, GO is considered as a catalyst support material for the intercalation of catalytically active transition and noble metal nanoparticles.

Graphite, inexpensive and available in large quantity, is widely used in heterogeneous catalysis, but there is little information available for DMC synthesis. In our previous work [38], carbonaceous materials (GO, expanded graphite, activated carbon and carbon nanotubes) supported Cu–Ni bimetallic catalysts have been prepared and applied successfully to the direct synthesis of DMC from CH_3OH and CO_2. From the study, it has been shown that the obtained catalysts exhibited higher catalytic performances than the traditional ones. We report herewith the preparation of GO supported Cu–Ni bimetallic catalysts using conventional wetness impregnation method, and the application of the as-made catalysts for the direct synthesis of DMC. This is a first demonstration that GO can be effectively used as catalyst support for the direct synthesis of DMC.

2. Experimental

2.1. Sample preparation

Natural graphite powder (NGP) ($C > 99\%$, $D = 5\ \mu m$) was used as precursor. NGP was firstly treated with 5% HCl twice, followed by filtering and washing with deionized water several times until neutral, and dried at 90 °C for 24 h. The GO used in this research was synthesized from the graphite by graphite oxidation with $KMnO_4$ in concentrated H_2SO_4 according to modified Hummer's method [39]. The typical procedures were depicted as follows: a blend of pure NGP (10 g) and sodium nitrate (5 g) was added into cold (4 °C) concentrated H_2SO_4 (230 ml) cooled by ice-water bath. $KMnO_4$ (30 g) was added into the above solution gradually with vigorous stirring and kept the temperature of the mixture below 20 °C. The mixture was stirred at 35 ± 3 °C for 30 min; distilled water (460 ml) was slowly added to the above mixture to cause an increase in temperature to 98 °C, and this temperature was kept for 15 min. The reaction was terminated by the addition of a large amount of distilled water (710 ml) and appropriate volume of H_2O_2 (5%). The mixture was filtered, washed successively with 5% HCl completely until absence of SO_4^{2-} (detected with $BaCl_2$ aqueous solution). The synthesized GO was dried at 50 °C for 24 h and conserved in desiccator before use.

Cu–Ni/graphite nanocomposite catalyst was prepared by traditional wetness impregnation method. The synthesis approach for the nanocomposite is depicted in Fig. 1. $Cu(NO_3)_2{\cdot}3H_2O$ and $Ni(NO_3)_2{\cdot}6H_2O$ were used as metal precursors. Prior to impregnation GO was firstly subjected to disperse in ammonia solution by ultrasonic vibration for 30 min. Simultaneously, $Cu(NO_3)_2{\cdot}3H_2O$ and $Ni(NO_3)_2{\cdot}6H_2O$ were dissolved in ammonia solution by stirring. Then copper and nickel ammonia solution was added to the GO colloidal solution under vigorous stirring. The resulting mixture was stirred at ambient temperature for 24 h, ultrasonicated for 30 min, and finally aged for 24 h, followed by rotavaporation to eliminate the solvent. Thereafter, the residual mixture was dried at 90 °C until the weight was unchanged. Upon completion, the fully dried product was crushed carefully in an agate mortar to give the catalyst precursors (CuO–NiO/GO), which were then calcined in N_2 flow (30 ml/min) at 400 °C for 2 h with a heating rate of 0.5 °C/min, and further reduced by 5% H_2/N_2 mixture under 600 °C for 2 h with a heating rate of 0.5 °C/min.

2.2. Characterization

2.2.1. BET measurement

Nitrogen adsorption/desorption isotherms were determined by N_2 physisorption in liquid N_2 (77 K) using a Micromeritics

Fig. 1. Schematic illustration of Cu–Ni/graphite nanocomposite catalyst synthesis.

ASAP 2010 instrument. The Brunauer–Emmett–Teller (BET) and the Barrett–Joyner–Halenda (BJH) approaches were used to determine the surface area and the pore size distribution of samples, respectively. Prior to analysis, the sample was outgassed at 523 K for 8 h in a stream of helium. The range of relative pressures (P/P_0) varied from 0.0009 to 1 and the equilibration time was 30 s.

2.2.2. Raman, FTIR spectra and TG–DSC study

Raman spectra of samples (4000–50 cm^{-1}) were recorded on Renoshaw inVia instrument. FTIR spectra of samples (4000–400 cm^{-1}) were recorded on an Analect RFX-65A type FTIR spectrophotometer. The spectra were recorded using the KBr pellets containing 0.1% of sample. These pellets were dried under infra light before the spectra were recorded. Thermogravimetric (TG–DTG) analyses of samples were performed on a PerkinElmer Pyris Diamond SII thermal analyzer. The samples were loaded into a china pan and heated under a high-purity N_2 flow from ambient temperature to 110 °C at a heating rate of 20 °C/min, held at this temperature for 20 min, and then increased temperature to 700 °C with a controlled heating rate of 10 °C/min. Differential scanning calorimeter (DSC) analysis was carried out in a flow of air at temperature ramping rate of 10 °C/min using Seiko 220 thermal analyzer. The sample loading was typically 30 mg.

2.2.3. Scanning electron microscopy (SEM)

The morphologies and microstructure of GO and metal particles were examined using a scanning electron microscopy (JSM-5600LV system of JEOL) equipped with an energy dispersive X-ray detector (EDX). The accelerating voltage was 15 kV.

2.2.4. Transmission electron microscopy (TEM)

The morphology, size and size distribution of Cu, Ni particles dispersed on the surface and interlayer of graphite were examined by transmission electron microscopy (JSM-2010 system of JEOL). The accelerating voltage was 200 kV. Sample preparation for TEM examination involved the ultrasonic dispersion of the sample in ethanol and placing a drop of the suspension on a copper grid, followed by solvent evaporation. Several TEM micrographs were recorded and analyzed for particle size distribution. At least 100 metal nanoparticles per sample were analyzed to determine their sizes and size distributions.

2.2.5. Powder X-ray diffractive (XRD)

XRD patterns of samples were recorded on a D/Max-IIIA power diffractometer in a step mode between 3° and 60° using Cu Kα radiation (0.15406 nm), operated at 35 kV and 25 mA. The intensity data were collected over a 2θ range of 3–60° with a 0.02° step size and using a counting time of 1 s per point. The average crystallite sizes were estimated by XRD line-broadening with the help of the Debye–Scherrer equation.

2.2.6. Temperature programmed reduction (TPR)

TPR experiments of calcined catalyst precursors were carried out using Quantachrom ChemBET 3000 apparatus. Samples were subjected to degassing pretreatment at 250 °C for an hour at helium flow (70 ml/min), and then cooled to room temperature. Thereafter, 10 mg of sample was placed in a quartz U-shaped tube, heated to 800 °C in a flow system using 5% H_2/He atmosphere (70 ml/min) with 8 °C/min temperature ramp. The signals of H_2 consumption by the sample, as a consequence of the temperature rise, were continuously monitored by a thermal conductivity detector (TCD).

2.2.7. X-ray photoelectron spectrum (XPS)

X-ray photoelectron spectrum of sample was obtained by using an ESCALAB 250 (Thermo-VG Scientific) analyzer. The used Al (Kα) radiation (1486.6 eV, 15 kV, and 150 W) was monochromatized. Survey scan spectra in the 1100–0 eV binding energy range were recorded with pass energy of 20.0 eV.

2.3. Direct synthesis of DMC from CH_3OH and CO_2

The catalytic activity of synthesized Cu–Ni/graphite nanocomposite catalyst for synthesis of DMC from CH_3OH and CO_2 was evaluated using a continuous tubular fixed-bed micro-gaseous reactor. The setup's configuration used for DMC synthesis was illustrated schematically in Fig. 2. The setup comprised of a micro-gaseous reactor (with photo or without photo, it could be selected freely), a CO_2 mass flow controller, a HLPC syringe pump, a six-way valve, a back-pressure regulator and a gas chromatography (GC). The six-way valve was placed into an oven. The oven, heater and reactor were each equipped with a thermometer, measured by thermocouples with an accuracy of ±1 °C. The system pressure was determined by pressure sensor and controlled by the back-pressure regulator with an accuracy of ±0.01 MPa.

A representative procedure is as follows: 1 g of fresh catalyst was first loaded into the reactor and the reactor was sealed and purged using CO_2 gas flow for 10 min to exhaust the air inside. Prior heating up CO_2 was charged into the reactor to a certain pressure and the flow rate was measured and controlled by the mass flow controller. When the heater, reactor and oven were heated to the desired temperature, the methanol was pumped into the system by the HPLC syringe pump. A 2:1 ratio of CH_3OH and CO_2 was kept during the reaction, which was controlled via vaporization temperature of CH_3OH and the flux of CO_2. Amounts of CH_3OH and CO_2 were controlled by gas-flow meter.

The catalytic reaction was carried out at different temperatures (353–413 K) and different pressures (0.4–1.6 MPa). The resulting mixture was introduced into the on-line GC (GC7890F) equipped with a flame ionization detector to analyze the composition and concentration. The condensed liquid from the cut-off valve was collected and analyzed by the gas chromatograph mass spectrometer (GCMS-QP2010 plus) to confirm the DMC formation in the reaction system. Catalyst activity is indicated by the CH_3OH conversion, DMC selectivity and DMC yield. These parameters are calculated according to the following equations:

$$\text{CH}_3\text{OH conversion}\,(\%) = \frac{[\text{CH}_3\text{OH reacted}]}{[\text{CH}_3\text{OH total}]} \times 100 \quad (1)$$

$$\text{DMC selectivity}\,(\%) = \frac{[\text{DMC}]}{[\text{DMC}] + [\text{by-products}]} \times 100 \quad (2)$$

$$\text{DMC yield}\,(\%) = \text{CH}_3\text{OH conversion} \times \text{DMC selectivity} \times 100 \quad (3)$$

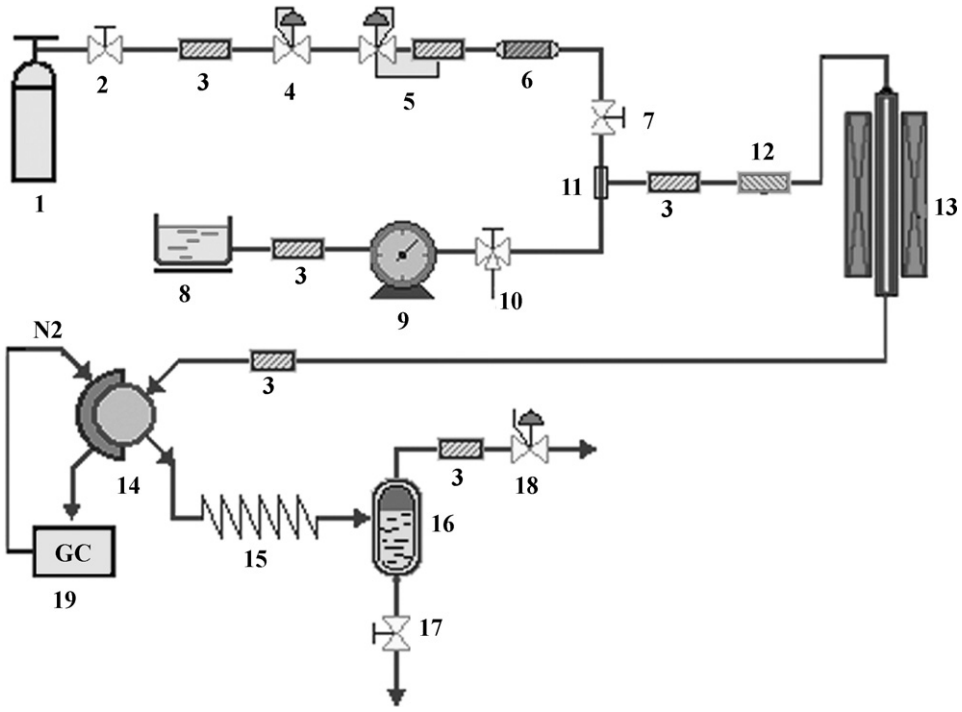

Fig. 2. Schematic diagram of apparatus for direct synthesis of DMC. (1) CO_2 cylinder; (2) pressure reducer valve; (3) filter; (4) pressure regulator; (5) mass flow controller; (6) buffer; (7) one-way valve; (8) methanol carrier; (9) HLPC syringe pump; (10) three-way inlet wave; (11) blender; (12) heater; (13) photo-reactor; (14) six-way valve; (15) cooler; (16) cooling separator; (17) cut-off valve; (18) back-pressure regulator and (19) gas chromatography.

3. Results and discussion

3.1. Synthesis of DMC from CH_3OH and CO_2

3.1.1. Effects of total metal content and molar ratio in Cu–Ni/graphite catalyst on the DMC synthesis

Table 1 shows the effects of total metal content and molar ratio in Cu–Ni/graphite catalyst on the DMC synthesis. The total metal content in the catalyst varied from 0 to 30 wt.%, and Cu/Ni ratio ranged from 1/5 to 5/1. For comparison, the catalytic activities of Cu/graphite and Ni/graphite monometallic catalysts were investigated. According to the experimental results, when no metal was loaded on graphite, the reaction did not take place at all (see Table 1, entry 1). With an increase in metal content, activity was found to generally increase (see Table 1, from entry 2 to 10). When metal content reached 20 wt.% and Cu/Ni ratio reached 2/1, Cu–Ni/graphite catalyst showed the best catalytic activity. Therefore, a total loading of metal 20 wt.% (CuO + NiO) and the molar ratio of 2/1 (Cu/Ni) were used in the optimized catalytic system. Interestingly, when Cu/graphite monometallic catalyst or Ni/graphite monometallic catalyst was alone used in the reaction, it could be seen that the activity was very low (Table 1, entries 19 and 20). However, when bimetallic catalyst was used in the reaction system, the activity was promoted obviously under given metal content and molar ratio. For example, the conversion of CH_3OH increased to 10.13% over the Cu–Ni/graphite bimetallic catalyst system (nearly four times of that over Cu/graphite alone). This was perhaps due to the synergetic effects of Cu, Ni and Cu–Ni alloy in the activation of CH_3OH and CO_2. These results will be further confirmed by the following experiments.

Table 1
The dependence of CH_3OH conversion and DMC selectivity on the loading and molar ratio of metals in the catalysts.[a]

Entry	(CuO + NiO) (%)	Cu:Ni molar ratio	CH_3OH conversion (%)	DMC selectivity (%)
1	0	0	None	None
2	5	5:1	3.96	85.4
3	5	3:1	4.01	86.6
4	5	2:1	4.57	89.3
5	5	1:1	4.18	91.2
6	5	1:2	3.64	92.0
7	8	2:1	5.16	91.1
8	10	2:1	6.38	90.7
9	15	2:1	8.96	90.4
10	20	2:1	10.13	90.2
11	21	2:1	9.38	88.8
12	25	2:1	9.24	88.1
13	30	2:1	7.73	85.8
14	20	3:1	9.22	87.2
15	20	5:1	7.91	83.1
16	20	1:1	6.60	88.3
17	20	1:2	6.11	89.6
18	20	1:3	5.09	91.9
19[b]			2.51	92.3
20[c]			0.79	91.1

[a] Reaction conditions: $n(CH_3OH)/n(CO_2) = 2/1$, catalyst weight 1.0 g, $P = 1.2$ MPa, $T = 100\,^{\circ}C$.
[b] Only Cu was loaded on the catalyst.
[c] Only Ni was loaded on the catalyst.

3.1.2. Effects of catalytic reaction conditions

The catalytic performance of Cu–Ni/graphite bimetallic nanocomposite catalyst in direct synthesis of DMC from CH_3OH and CO_2 was evaluated in a micro-reactor. To our delight, the prepared Cu–Ni/graphite bimetallic nanocomposite catalyst can efficiently catalyze the direct synthesis of DMC. It has been reported that the temperature and pressure affect the catalytic reaction considerably [10–12]. In this paper, these two factors were investigated. Catalytic reaction was carried out at different temperatures in a range of 353–403 K and different pressures in a range of 0.8–1.5 MPa. The results are summarized in Fig. 3. Fig. 3(a) shows the temperature dependence of DMC synthesis under a

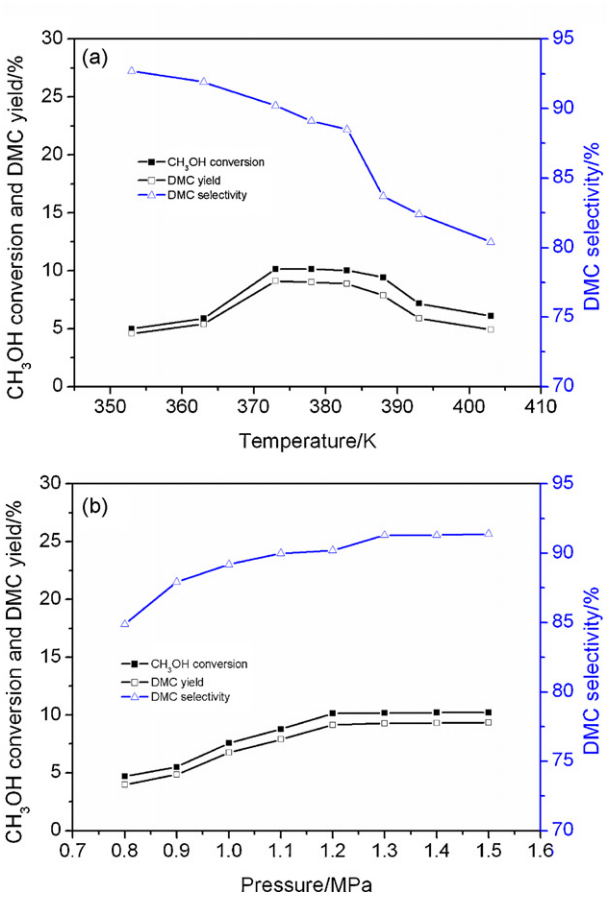

Fig. 3. The dependence of CH_3OH conversion, DMC yield and selectivity on temperature (a) and pressure (b) over Cu–Ni/graphite nanocomposite catalyst.

constant pressure of 1.2 MPa. Obviously, temperature has great effect on the DMC synthesis. The CH_3OH conversion and DMC yield increased with increasing temperature from 353 to 378 K and reached a peak value (10.13% of CH_3OH conversion and 9.02% of DMC yield) at 378 K, then decreased when temperature went up to 403 K. This indicated that the optimized temperature was 378 K. The activation of CH_3OH and CO_2 was more favorable when temperature increased, however, the DMC yield decreased dramatically at temperature above 378 K, likely due to the decreased CO_2 adsorption on catalyst at high temperature. Selectivity of DMC dropped slowly when temperature was lower than 383 K. When temperature was higher than 383 K, the selectivity decreased more dramatically, probably due to the decomposition of DMC at higher temperature. In summary, under the optimal reaction conditions of 1.2 MPa and 378 K DMC yield of 9.02% with the DMC selectivity of 89.1% were obtained using the supported catalyst. The by-products are CO, CH_4, dimethyl ether (DME) and H_2O. Presumably, CO is resulted from the cleavage of the C–O bond of the CO_2^- species, CH_4 comes from the activation species of CH_3OH, while DME is produced via the reaction between methoxy anion (CH_3O^-) and methylic species (CH_3^+), which are the main activated species of CH_3OH by the catalyst.

Pressure also played an important role in the reaction. Fig. 3(b) illustrates the pressure dependence of DMC synthesis. The CH_3OH conversion, DMC yield and selectivity were enhanced when the pressure increased from 0.8 to 1.5 MPa. DMC yield increased more than 2.3 times (from 3.98% of 0.8 MPa to 9.33% of 1.4 MPa), and selectivity of DMC also improved from 84.9 to 91.3%. The increasing trend of DMC yield levelled off when the pressure reached 1.2 MPa

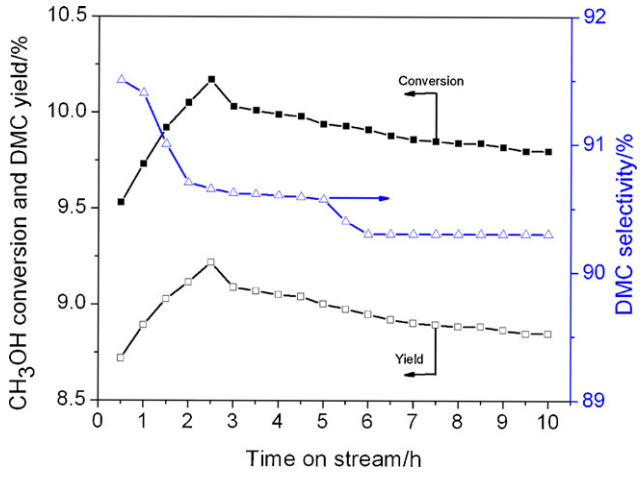

Fig. 4. Stability of the Cu–Ni/graphite nanocomposite catalyst (reaction conditions: T = 383 K; P = 1.2 MPa; catalyst weight: 1 g; and CH_3OH/CO_2 (molar ratio) = 2:1). (■) CH_3OH conversion; (□) DMC yield; (△) DMC selectivity.

(from 9.03% of 1.2 MPa to 9.33% of 1.6 MPa), indicating higher pressure would have no significant effect on the reaction.

3.1.3. Stability test results of catalyst

The catalyst test was continued for 10 h to examine the stability of the catalyst. The reaction was carried out at 378 K and under 1.2 MPa. The CH_3OH/CO_2 molar ratio was controlled to be 2:1, and 1 g catalyst was used. Fig. 4 shows CH_3OH conversion, DMC yield and DMC selectivity as a function of reaction time. It was found that CH_3OH conversion decreased slowly from 10.17 to 9.80%, the yield of DMC decreased from 9.21 to 8.84%, and the selectivity of DMC decreased from 91.5 to 90.3%. The increased activity observed at a reaction time of 0.5–3 h was likely due to the formation of active species in the initial reaction stage. The decreasing trend of CH_3OH conversion and DMC yield levelled off after 3-h reaction. The continuous decrease in catalyst activity indicated that deactivation of the composite catalyst proceeded gradually. Deactivation of catalyst in the DMC synthesis process is likely due to a change in oxidation state of metal. In addition, the increase of metal particles size may be another factor contributing to the deactivation. Since the active phases of the catalyst were metal phase of Cu, Ni and Cu–Ni alloy, the changes in oxidation state and an increase in metal particle size could result in the decrease in activity. These findings indicate that the deactivated catalyst can be easily regenerated by simple calcination and pre-reduction, leading to the re-dispersion of metal species, formation of the metal phases and recovery of the catalytic activity. The catalyst developed in this study exhibited fairly good durability as well as activity in direct synthesis of DMC under given experimental conditions. Companied with the advantages including of high catalytic performance, low cost, large-scale availability and readily regeneration, the catalyst developed in this work will show a great potential in DMC industrialisation.

3.2. Investigation of support and catalyst structure

After oxidation, the black slurry of NGP became orange (yellow), indicating the formation of GO [37]. The oxidation result of NGP was confirmed by elemental analyses (PerkinElmer 2400 series I CHNS/O analyzer), as the C/O ratio has been used as a conventional measure of the oxidation degree of graphitic materials. The C/O in GO was 4/2.4. BET measurement of GO at −196 °C indicated that the dominate mesopores ranging from 30 to 100 nm were mainly contained within GO structure besides a small quantity of

micropores with the size of 10–30 nm (Figure SM 1, see Supplementary Material). In the Raman spectrum of GO and Cu–Ni/graphite (Figure SM 2, see Supplementary Material), the prominent features of graphitic materials were the well-known D and G bands. The sharp D band at 1599 cm^{-1} and G band at 1349 cm^{-1} showed the defective, crystalline structure of graphene nanosheets [40–42]. Compared with GO, the D band and G band of catalyst had a negative shift (from 1599 to 1588 cm^{-1} and from 1349 to 1355 cm^{-1}, respectively), indicating that some changes in the support surface had taken place after impregnation. And also, reduction of catalyst had somewhat effect on the structure and surface of graphite. In the FTIR spectrums (Figure SM 3, see Supplementary Material), no peak was found on NGP. GO showed four sharp peaks, 3431, 1714, 1625, and 1045 cm^{-1}, which corresponded to –OH, C=O, free water and C–O–C group, respectively [43,44]. In contrast, for Cu–Ni/graphite catalyst, the peaks of C=O and C–O–C were absent, and a new peak at 1467 cm^{-1} appeared. These changes implied that some interactions were established between the metal precursors and the supports in the impregnation, and also supported the reduction of GO and the partial removal of the oxygen functional groups. In the TG–DTG–DSC profiles of GO (Figure SM 4, see Supplementary Material), GO exhibited a major weight loss around 200 °C (The weight loss between room temperature and 200 °C was 19.0%), which was attributed to the removal of organic groups, while the weak weight loss below 100 °C was due to the physically adsorbed water. This result was similar to the high adsorbed water content observed by Bourlinos et al. [45]. DSC of GO showed one strong extherthomic peak at 204 °C, which was caused by the decomposition of organic groups on GO sheets. FTIR and TG results implied that the prepared GO had well hydrophilicity, which allowed GO to readily swell and exfoliate in water. This specific surface characteristic of GO was very important to prepare GO supported catalyst, for if the hydrophilicity of the support increased remarkably, the deposition of active metal would be very profitable in the aqueous solution. It is generally accepted that the dispersion of active metal particles on the support surface is a critical parameter for catalytic activity. Therefore, the changes in surface properties of supports will have positive effects on the morphology and, consequently, to final catalytic activities of catalysts.

The typical SEM images of samples are shown in Fig. 5. Although the layered structure of pristine NGP was maintained well in GO, the value of the gallery spacing (0.335 nm) among carbon nano-sheets

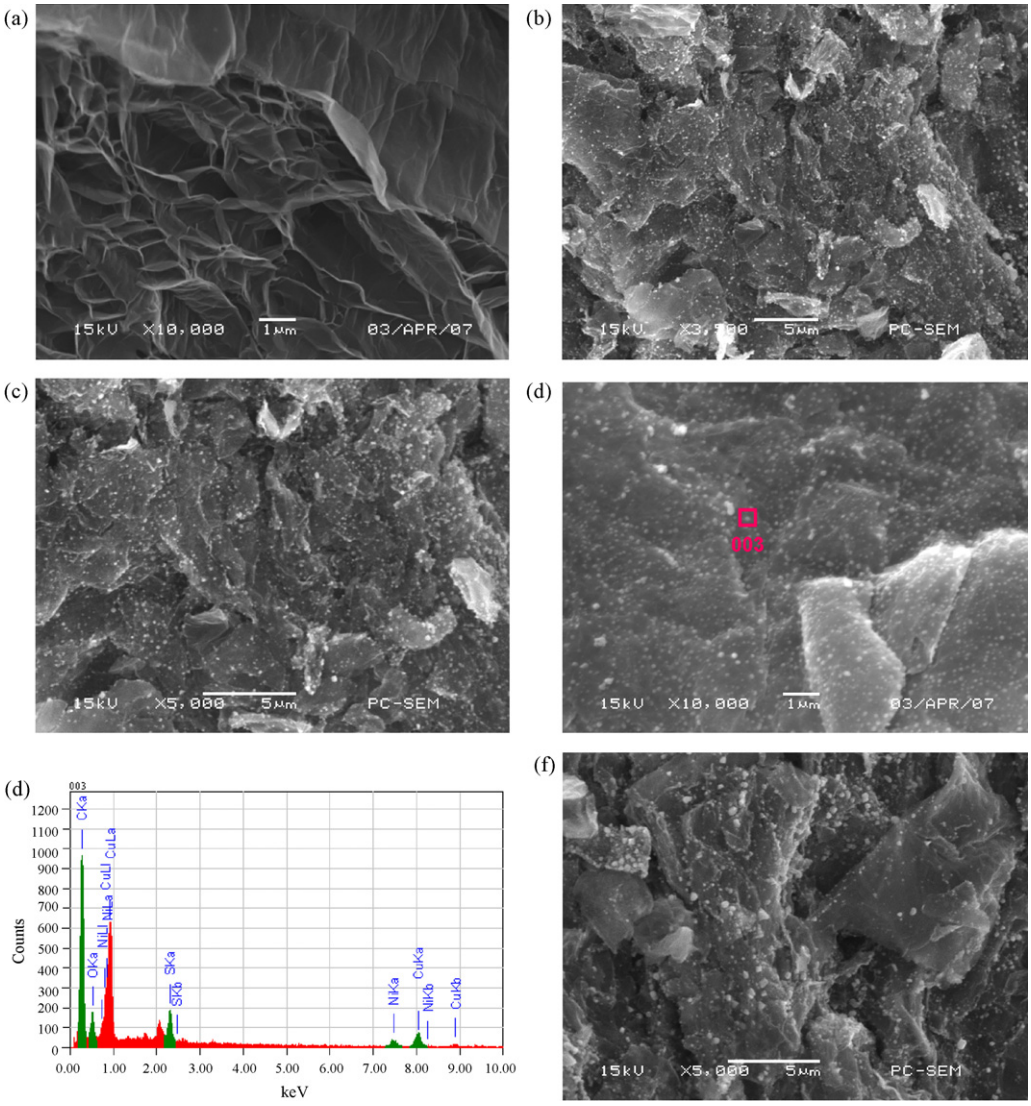

Fig. 5. SEM images of samples. (a) GO; (b) fresh Cu–Ni/graphite nanocomposite catalyst (3.5k×); (c) fresh Cu–Ni/graphite nanocomposite catalyst (5.0k×); (d) fresh Cu–Ni/graphite nanocomposite catalyst (10.0k×); (e) EDX of (d) and (f) deactivated catalyst after 10-h reaction (5.0k×).

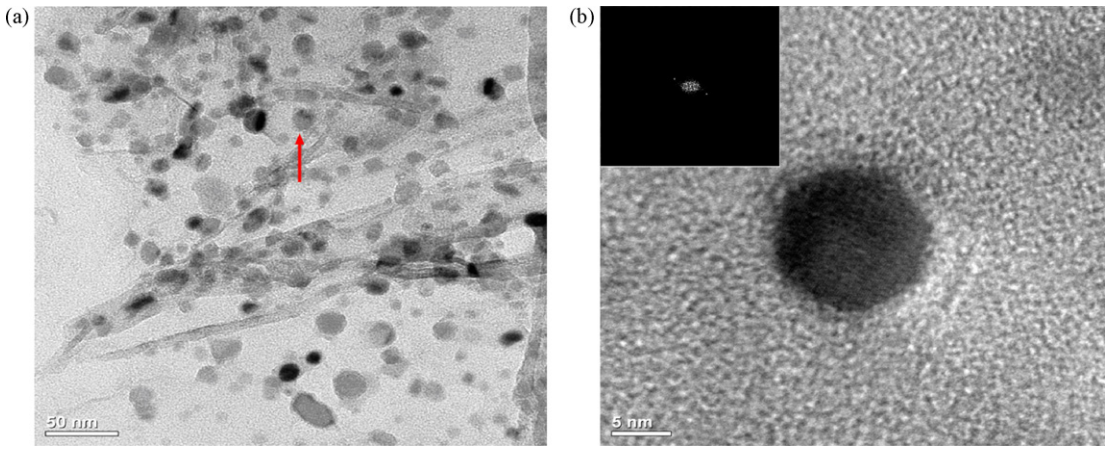

Fig. 6. TEM images of (a) Cu–Ni/graphite nanocomposite catalyst and (b) the magnification image of a selected metal particle (as the arrow shown in a), the inset image is the diffractogram mode of metal particle of (b).

increased because H_2O molecules and oxygen-containing functional groups were intercalated into the layer of graphite (Fig. 5(a)). Fig. 5(b)–(d) shows the SEM images of the fresh catalyst at different magnification. It was evident that active metal particles (white circular dot) were evenly dispersed in/on the lamellae or surface of GO, meanwhile, the interlayer spacing among the carbon sheets was expanded compared to that of original NGP (the SEM image of NGP was not shown here). This was attributed to two factors. Firstly, Cu^{2+} and Ni^{+} were intercalated into the lamellae of GO to get an extended interlayer spacing under the cooperative effect of adsorption and ion-exchange in the process of wet impregnation; furthermore, GO layers could be exfoliated or delaminated when subjecting to stirring and ultrasonic force, this force could accelerate the intercalation and dispersion of Cu^{2+} and Ni^{+} thoroughly. This explanation could be further confirmed by the results of XRD measurement. The energy dispersive X-ray detector (EDX) suggested that these white circular dots include Cu, Ni elements (Fig. 5(e)). Fig. 5(f) shows the SEM image of catalyst after 10-h reaction, active metal particles in this image were uneven in size and exhibited some aggregation. Further observation indicated that this sample presented the broadest size distribution for active metal particles. The increase in active metal particles size could be one of the reasons for catalyst deactivation, as discussed in the former section.

TEM is a powerful technique to gain insight into morphology and microstructure of catalysts. Fig. 6 presents the TEM observations of Cu–Ni/graphite catalyst and the corresponding selected area electron diffraction pattern of the metal particle. Some differences in the size and morphological characteristic of metal particles on the catalyst could be observed (Fig. 6(a)). From a survey of many areas of the specimen, it was evident that metal particles were evenly distributed over the graphite surface, and generally, the particles adopted with spherical, rectangle and cubic shapes. As shown in the electron diffraction pattern (inset image in Fig. 6(b)), the crystallinity of the metal particle (as the arrow shows in Fig. 6(a) and the corresponding magnification image in Fig. 6(b)) on graphite was maintained well because the planar crystal lattice diffraction could be observed. The diameter distribution of metal particles was in range from 5 to 25 nm and the average size of these particles was 15.8 nm by TEM image analysis.

The XRD patterns of samples are displayed in Fig. 7. After oxidation, the graphitic (0 0 2, $2\theta = 26.6^\circ$ and 0 0 4, $2\theta = 54.8^\circ$) diffraction peaks (Fig. 7(a)) completely disappeared and, instead, were replaced by a well-defined peak at a lower diffraction angle (Fig. 7(b), $2\theta = 13.0^\circ$), which corresponded to and interplanar distance of 0.858 nm. The absence of the characteristic 0 0 2 diffraction of graphite at 26.6° confirmed the completion of oxidation [46], resulting in the formation of a well-ordered, lamellar structure, which was more open than that of graphite (0.335 nm) and thus more susceptible to intercalation [46]. The increase of basal spacing of GO in the course of oxidation owing to the expansion of the layer planes caused by accommodation of various oxygen species and the changes of carbon hexahedron grid plane during oxidation [47]. The interlayer spacing of GO (0.858 nm) was in the range of the reported values (0.6–1.1 nm) [48]. The weak peak at $2\theta = 20.6^\circ$ indicated the existence of some stacking structures. After being reduced by H_2 (Fig. 7(c)), the diffraction peak of GO disappeared and the graphitic (0 0 2) diffraction peak appeared again although not as sharp as the original graphite, indicating that the structural of GO was changed during the reduction. The interlayer distance ($2\theta = 26.6^\circ$) of the nanocomposite catalyst was 0.338 nm, which was larger than that of NGP (0.335 nm) owing to the existence of

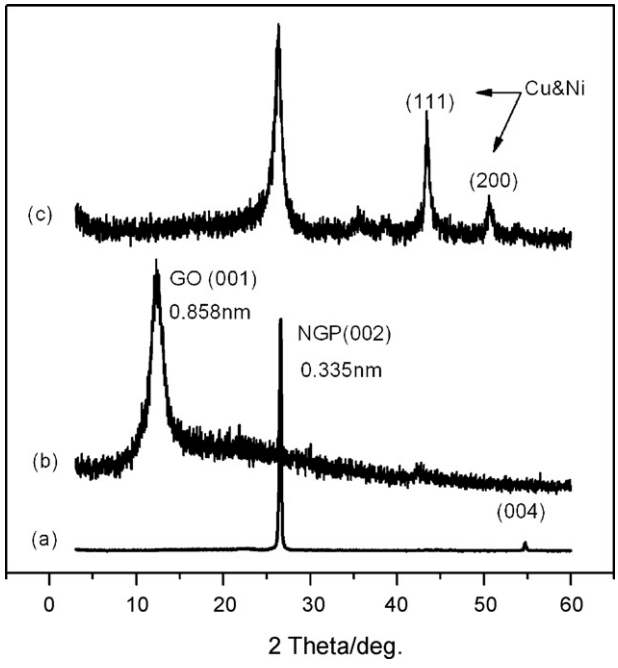

Fig. 7. XRD patterns of (a) NGP; (b) GO and (c) Cu–Ni/graphite nanocomposite catalyst.

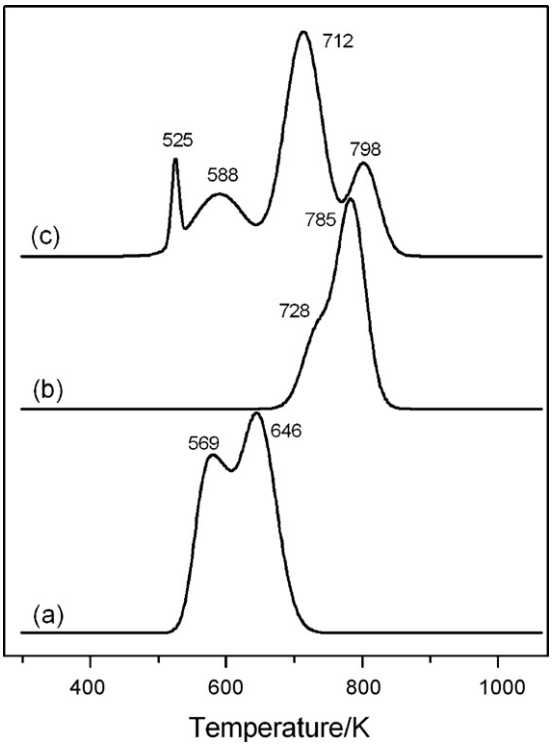

Fig. 8. TPR profiles of calcined catalyst precursors. (a) CuO/graphite; (b) NiO/graphite and (c) CuO–NiO/graphite.

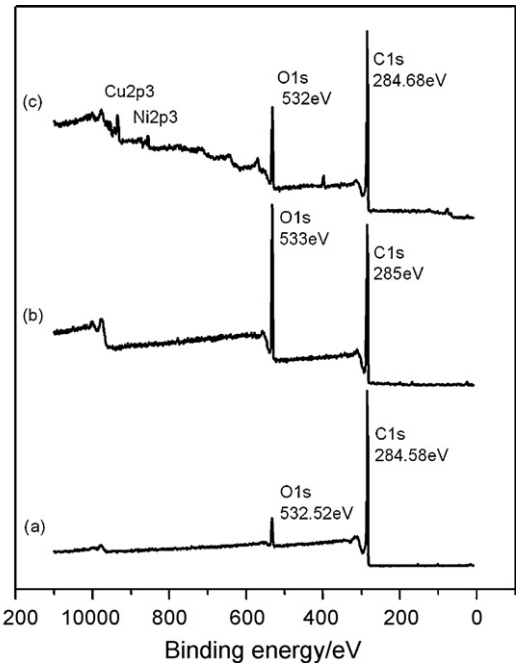

Fig. 9. XPS patterns of (a) NGP; (b) GO and (c) Cu–Ni/graphite nanocomposite catalyst.

small quantity of O bonded in the graphite layer. For the XRD of Cu–Ni/graphite (Fig. 7(c)), two new diffraction peaks at $2\theta = 43.4^\circ$ (1 1 1) and 50.7° (200) appeared, which could be assigned to diffraction of metal phase Cu and cubic phase Cu–Ni alloy. XRD results indicated that metallic phases of Cu, Ni and alloy phase of Cu–Ni were formed in reduction and activation step.

H_2-TPR is a useful characterization technique for investigating the chemical properties of a metal catalyst. TPR can reveal not only the reducibility and stability of the metal-supported or unsupported catalysts, but also the more profound surface chemical information, that is, metal species, metal distribution, and, even quantitatively, the loading of different metal surface forms. The TPR profiles of different samples are presented in Fig. 8. For comparative purpose, the TPR of CuO/graphite and NiO/graphite monometallic catalyst precursors were also characterized. It could be seen that the CuO/graphite showed a main reduction peak at 646 K and a shoulder peak at 569 K, respectively (Fig. 8, trace a). The main peak was related to a two-step reduction of CuO to Cu_2O and Cu_2O to Cu, while the shoulder peak corresponded to the reduction of the well-dispersed CuO species. For the reduction of NiO/graphite, the TPR profile showed only one distinct peak (accompanied by a weak shoulder peak) in the range of 700–850 K, indicating that the sample was likely to have a single species on the surface (Fig. 8, trace b). The main reduction peak observed at 785 K was related to the reduction of NiO to Ni, while the weaker shoulder peak detected at 728 K corresponded to the reduction of the well-dispersed NiO species. Notably, the reduction temperatures of CuO and NiO species were higher than those of bulk CuO (503 K) and NiO (703 K), respectively [49], which was attributed to the interaction between metal oxides and graphite. The TPR profiles of CuO–NiO/graphite sample showed four reduction peaks (Fig. 8, trace c). The peaks detected at 525 and 588 K were related to the reduction of CuO species. The peak observed at 798 K was ascribed to the reduction of NiO species. A distinct peak observed at 712 K, differed from that of reduction of CuO and NiO, was likely corresponded to the reduction of CuO–NiO compounds. According to the XRD results, CuO–NiO compounds changed into Cu–Ni alloy during the reduction and activation step.

The samples were further analyzed by XPS to determine the oxidative state of Cu and Ni and the interactions between metal particles and graphite. Fig. 9 shows the XPS patterns of various samples. The survey scan spectra indicated the presence of C and O atoms on the surface of both samples (curves a–c). The oxygen content of GO was much higher due to the oxidative treatment, while for graphite it could be explained by a slight atmospheric oxidation. For comparison, the binding energy levels of C 1s, O 1s were displayed in Fig. 9. It could be found that the binding energy of C 1s and O 1s for NGP stayed at the normal value of 284.58 and 532.52 eV, respectively (Fig. 9(a)). However, they shifted to 285 eV of C 1s and 533 eV of O 1s for GO (Fig. 9(b)). The 0.42 and 0.48 eV positive shifts, presumably due to the changes of chemical environments on graphite surface (owing to introduction of some oxygen functional groups such as hydroxyl and epoxide groups). After being reduced by H_2, the binding energy shift for C 1s and O 1s, from 285 to 284.68 eV of C 1s and 533 to 532 eV of O 1s in Cu–Ni/graphite (Fig. 9(c)) could be observed. The slightly negative shift was attributed to the reduction of GO. The Cu ($sp_{2/3}$) and Ni ($sp_{2/3}$), located at 932.8 and 853.5 eV, respectively, were slightly different from those reported in literature [49]. These differences indicated that some changes in electron density and chemical environmental of Cu and Ni took place in catalyst preparation. Presumably, it was due to the interactions between Cu, Ni metals and graphite, as well as the formation of Cu and Ni alloy. These results could be confirmed by results of XRD and TPR.

4. Proposed reaction mechanisms

Based on the experimental results of this work and that of literatures [50–52], a catalytic cycle for the direct synthesis DMC from CH_3OH and CO_2 using the catalyst can be proposed in Fig. 10. M is Cu or Ni or Cu and Ni alloy. The catalytic cycle has three steps: (i) activation of CH_3OH on M surface to form CH_3O-species; (ii) activation of

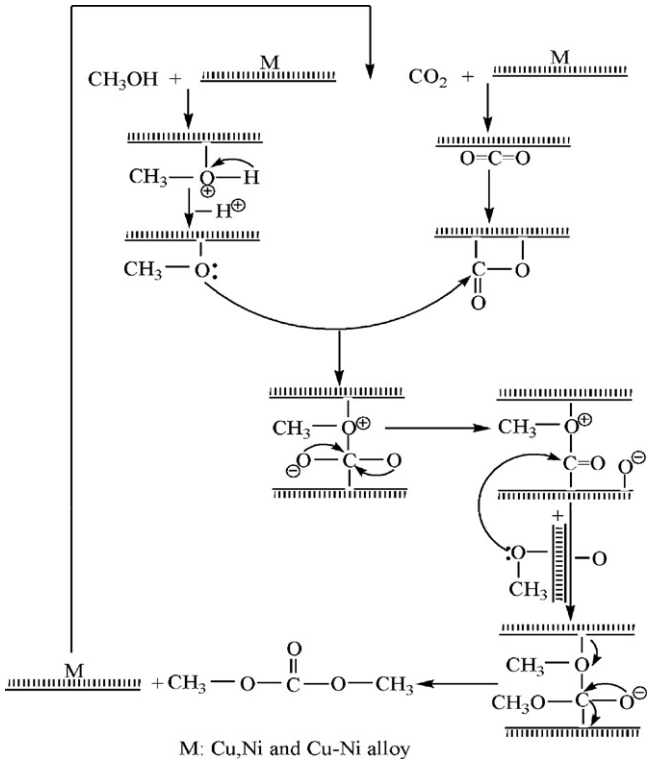

Fig. 10. Possible catalytic mechanism for direct synthesis DMC from CH_3OH and CO_2 over Cu–Ni/graphite nanocomposite catalyst.

CO_2 on M surface to form —C═O species, and (iii) reactions between the resulting CH_3O— species and —C═O species leading to DMC and regeneration of M. Electron transfer might play an important role in the activation of reactants and formation of DMC. Selection of a suitable supporting material with extraordinary electronic transport properties will likely favor the reaction.

Although the mechanism of the reaction is not well understood, especially for the activation mechanism of reactant over the synthesized catalyst, it is believed that the synergetic effects of metal Cu, Ni and Cu–Ni alloy in the activation of CH_3OH and CO_2 likely play a significant role. Moreover, the characteristics and structure of graphite could be very important. GO is multifunctional inorganic material with many functional groups and loose carbon sheets, which may facilitate the dispersion of copper and nickel atoms, leading to higher surface area of active metal. Moreover, the graphite sheets have extraordinary electronic transporting properties and high electronic conductivity, and may induce electronic perturbations in the metallic components, changes the electronic balance of metal-support system, and thus improves metal-support interaction, and affect the reactivity and selectivity of chemical reactions. Moreover, low carbonic electro-negativity of graphite makes electrons in the graphite can be released easily, which is a key factor in the activation of CO_2.

5. Conclusions

Based on the experimental results, we draw the following conclusions:

(1) Cu–Ni/graphite catalysts are effective in direct synthesis of DMC from CH_3OH and CO_2. Under the optimal reaction condition of 378 K and 1.2 MPa, the highest DMC yield was higher than 9.0% and the selectivity of DMC was higher than 88.0%.

(2) Cu–Ni alloy was formed partly in the reduction and activation step. Metal phase of Cu, Ni and Cu–Ni alloy co-existed in the synthesized catalyst. The synergetic effects of metal Cu, Ni and Cu–Ni alloy played an important role in the activation of CH_3OH and CO_2. In addition, the particular character of graphite, moderate Cu–Ni–graphite interactions, and the dispersing states of metal particles also contributed to the observed catalytic activity.

(3) Graphite as a novel support used widely in heterogeneous catalytic processes will trigger more intense research in catalytic synthesis of DMC. Further improvement in the DMC yield and acceleration of the reaction rate may provide a practical solution to CO_2 utilization. Compared to the scientific progress in direct synthesis of DMC reported by peers, the findings of this paper can be considered as a breakthrough.

Acknowledgements

The authors would like to thank Guangdong Province Sci & Tech Bureau (Key Strategic Project Grant No. 2006B12401006), and Guangzhou Sci & Tech Bureau (2005U13D2031, 2007Z2-D2031) for financial support of this work. Y.L. thanks National University of Singapore for financial support. The authors thank the China High-Tech Development 863 Program.

Appendix A. Supplementary data

Supplementary data associated with this article can be found, in the online version, at doi:10.1016/j.cej.2008.11.006.

References

[1] M. Aresta, E. Quaranta, Chemtech 27 (1997) 32–40.
[2] A.A. Shaikh, S. Sivaram, Chem. Chem. Rev. 96 (1996) 951–976.
[3] P. Tundo, G. Moraglio, F. Trotta, Ind. Eng. Chem. Res. 28 (1989) 881–887.
[4] Y. Ono, Appl. Catal. A 155 (1997) 133–166.
[5] P. Jessop, T. Ikariya, R. Noyori, Chem. Rev. 99 (1999) 475–494.
[6] D. Molzahn, M.E. Jones, G.E. Hartwell, J. Puga, US Patent 7,085,387 (1995).
[7] C. Jegat, J. Mascetti, M. Fouassier, M. Tranquille, M. Aresta, I. Tommasi, A. Dedieu, Inorg. Chem. 32 (1993) 1279–1289.
[8] C.S. Hwang, N.C. Wang, Mater. Chem. Phys. 88 (2004) 258–263.
[9] K. Tominaga, Y. Sasaki, J. Mol. Catal. A: Chem. 220 (2004) 159–165.
[10] X.L. Wu, M. Xiao, Y.Z. Meng, Y.X. Lu, J. Mol. Catal. A: Chem. 238 (2005) 158–162.
[11] X.L. Wu, M. Xiao, Y.Z. Meng, Y.X. Lu, J. Mol. Catal. A: Chem. 249 (2006) 93–97.
[12] X.J. Wang, M. Xiao, S.J. Wang, Y.X. Lu, Y.Z. Meng, J. Mol. Catal. A: Chem. 278 (2007) 92–96.
[13] J. Kizlink, Collect. Czec. Chem. Commun. 58 (1993) 1399–1402.
[14] J. Kizlink, I. Pastucha, Collect. Czech. Chem. Commun. 60 (1995) 687–693.
[15] S. Fang, K. Fujimoto, Appl. Catal. A 142 (1996) L1–L3.
[16] K. Tomishige, T. Sakaihiro, Y. Ikeda, K. Fujimoto, Catal. Lett. 58 (1999) 225–229.
[17] K. Taek Jung, T. Alexic Bell, Top. Catal. 20 (2002) 97–102.
[18] C.J. Jiang, Y.H. Guo, C.G. Wang, C.W. Hu, Y. Wu, E.B. Wang, Appl. Catal. A 256 (2003) 203–212.
[19] K.S. Novoselov, A.K. Geim, S.V. Morozov, D. Jiang, Y. Zhang, S.V. Dubonos, A.A. Firsov, Science 306 (2004) 666–669.
[20] K.S. Novoselov, A.K. Geim, S.V. Morozov, D. Jiang, M.I. Katsnelson, I.V. Grigorieva, S.V. Dubonos, A.A. Firsov, Nature 438 (2005) 197–200.
[21] Y. Zhang, Y.W. Tan, H.L. Stormer, P. Kim, Nature 438 (2005) 201–204.
[22] X.S. Du, M. Xiao, Y.Z. Meng, A.S. Hay, Synth. Mater. 143 (2004) 129–132.
[23] P. Colin, R. Baker, K.J. Terry, Phys. Chem. B 103 (1999) 2453–2458.
[24] D. Richard, P. Fouilloux, P. Gallezot, Proc. 9th. Int. Congr. Catal. 3 (1988) 1074–1081.
[25] I.C. Brownlie, J.R. Fryer, G.J. Webb, J. Catal. 14 (1969) 263–269.
[26] J. de Lopez-Gonzalez, A. Martin-Rodriguez, F. Dominguez-Vega, Carbon 7 (1969) 583–588.
[27] J.C. Bailar Jr., H.J. Emelus, S.R. Nyholm, A.F. Trotman-Dickenson, Comprehensive Inorganic Chemistry, Pergamon Press, Oxford, 1973.
[28] T. Nakajima, Y. Matsuo, Carbon 32 (1994) 469–475.
[29] A. Hamwi, V.J. Marchand, Phys. Chem. Solids 57 (1996) 867–882.
[30] A. Lerf, H. He, M. Forster, J. Klinowski, J. Phys. Chem. 102 (1998) 4477–4482.
[31] H. He, J. Klinowski, M. Forster, A. Lerf, Chem. Phys. Lett. 287 (1998) 53–56.
[32] N. Kovtyukhova, E. Buzaneva, A. Senkevich, Carbon 36 (1998) 549–554.
[33] P. Liu, K. Gong, P. Xiao, M. Xiao, J. Mater. Chem. 10 (2000) 933–938.

[34] E.L. Evans, J. de Lopez-Gonzalez, A. Martin-Rodriguez, F. Rodriguez-Reinoso, Carbon 13 (1975) 461–464.
[35] M. Hirata, T. Gotou, M. Ohba, Carbon 43 (2005) 503–510.
[36] M. Xiao, X.S. Du, Y.Z. Meng, New Carbon Mater. (Chin.) 19 (2004) 92–96.
[37] S. Stankovich, D.A. Dikin, G.H.B. Dommett, K.M. Kohlhaas, E.J. Zimney, E.A. Stach, R.D. Piner, S.T. Nguyen, R.S. Ruoff, Nature 442 (2006) 282–286.
[38] Y.Z. Meng, J. Bian, M. Xiao, F.G. Du, S.J. Wang, X.J. Wang, Y. Xu, CN Patent 1,011,433,22 (2008).
[39] W.S. Hummers, R.E. Offeman, J. Am. Chem. Soc. 80 (1958) l339–1339.
[40] E.C. Walter, T. Beetz, M.Y. Sfeir, L.E. Brus, M.L. Steigerwald, J. Am. Chem. Soc. 128 (2006) 15590–15591.
[41] J.J. Wang, M.Y. Zhu, R.A. Outlaw, X. Zhao, D.M. Manos, B.C. Holloway, V.P. Mammana, Appl. Phys. Lett. 85 (2004) 1265–1267.
[42] J.J. Wang, M.Y. Zhu, R.A. Outlaw, X. Zhao, D.M. Manos, B.C. Holloway, Carbon 42 (2004) 2867–2872.
[43] T. Szabo, O. Berkesi, P. Forgo, K. Josepovits, Y. Sanakis, D. Petridis, I. Dekany, Chem. Mater. 18 (2006) 2740–2749.
[44] X.S. Du, M. Xiao, Y.Z. Meng, A.S. Hay, Carbon 43 (2005) 195–197.
[45] A.B. Bourlinos, D. Gournis, D. Petridis, T. Szabo, A. Szeri, I. Dekany, Langmuir 19 (2003) 6050–6055.
[46] L.C. Hontoria, A.J. Lopez-Peinado, J. de Lopez-Gonzalez, M.L. Rojas-Cervantes, R.M. Martin-Aranda, Carbon 33 (1995) 1585–1592.
[47] M. Mermous, Y. Chabre, A. Roishall, Carbon 29 (1991) 469–474.
[48] J.W. Pechett, T. Philippe, Carbon 38 (2000) 345–349.
[49] A.R. Naghash, T.H. Etsell, S. Xu, Chem. Mater. 18 (2006) 2480–2488.
[50] I.E. Wachs, R.J. Madix, J. Catal. 53 (1978) 208–227.
[51] S.D. Jackson, J. Catal. 115 (1989) 247–249.
[52] H. Behner, W. Spiess, G. Wedler, D. Borgmann, Surf. Sci. 175 (1986) 276–286.